HEAT AND MOMENTUM TRANSPORT IN PLASMA FLOW AROUND A SOLID SPHERE

Mohamed M. Elafify, Hanaa H. Abou Gabal and Mofreh R. Zaghloul
Nuclear Engineering Department, Alexandria University
Alexandria, Egypt

ABSTRACT

The problem of heat and momentum transfer between a high temperature plasma and a small diameter spherical particle has been studied using a two-temperature, chemical, non-equilibrium approach, incorporating rarefaction and particle charging effects. The most important effects which are not present in ordinary gases such as, strongly varying plasma properties, dissociation, recombination, radiation and non-continuum situations has been taken into account in addition to the particle surface charging. A physical model is introduced to represent flow and energy transfer of heavy particles and electrons. A study was performed using the proposed physical model to determine the isotherms of both electrons and heavy particles, as well as, the pressure distribution, the drag coefficient, the tangential velocity, and the heat flux at the sphere surface for particles of diameter 20 micrometer immersed in 13,000 °K Argon plasma. The results of the heat flux are compared with Chen-Pfender's work [1]. It is concluded that the effect of departure of plasma from thermodynamic equilibrium should be taken into consideration nearby the sphere surface. To represent the flow field around a sphere, it is found that a domain of about twenty times the sphere radius is enough to simulate the boundary layer around the sphere. The one-fluid, one-temperature model [1] underestimates the heat fluxes from plasma to the sphere surface because it overlooks the contribution of electrons. Compared with Chen-Pfender's previous work [1] using one fluid one temperature model, the difference in calculated heat flux is about 20%.

Keywords: Plasma flow, Flow around solid spheres, Fluid flow equations, Finite difference.

INTRODUCTION

Thermal plasma processing offers interesting possibilities for the development of new technologies and for new processing routes. Thermal plasmas with temperatures typically in the order of 10,000 °K provide extremely high heating and quenching rates for particulate matter injected into such plasmas. Under these extreme conditions, unusual materials or coatings may be produced with interesting properties.

Particles injected into a thermal plasma will experience a number of effects which are not present in ordinary gases. Y.C.Lee, Y.P.Chyou and E.Pfender [2] described in a comprehensive review the most important effects which have to be considered. Some of the various effects which are known today are listed in Table (1) [2].

Table 1. Effects Involved in Particle Heat and Momentum Transfer in a Thermal Plasma [2].

(1) Internal conduction.
(2) Unsteady condition.
(3) Modified transfer coefficients due to strongly varying plasma properties.
(4) Non continuum effect.
(5) Radiation.
(6) Particle shape.
(7) Particle charging.

ESTABLISHMENT OF GOVERNING EQUATIONS

- *Internal Conduction*

The Biot number, defined as the ratio of convective to conductive heat transfer, serves as a criterion for determining the relative importance of heat conduction within a particle. If Bi<<0.1, internal conduction is relatively high, i.e., temperature variations within the particle are negligible.

Bourdin et al [3] proposed a method for calculating the Biot number assuming that conduction is the governing heat transfer mechanism (small Reynolds numbers) for particle heating in the plasma, i.e.,

$$Bi = \frac{\bar{K}}{K_p}$$

where $\bar{K}$ is the average thermal conductivity of the plasma across the boundary layer, and K_p is the thermal conductivity of the particle material . It is safer to take the upper limit of the critical Biot number of the particle during its flight as:

$$Bi_{crit} = 2 * \frac{K(T_{avg})}{K_p(T_{w,avg})}$$

Where a factor of 2 incorporates the convective influence; and thermal conductivities of the particle and the plasma are chosen with respect to estimated average temperatures.

Based on this criterion the internal conduction resistance of the particle is negligible if Bi_{crit}<<0.1. For this case, a simplified approach can be used to calculate heat and mass transfer.

- *Pseudo-Steady-State Situation*

If the temperature and velocity fields in the boundary layers surrounding a particle do not relax fast enough when the particle is exposed to drastically varying temperatures and velocities, then the so-called pseudo-steady-state conditions are not reached, i.e., steady-state expressions are not valid.

Bourdin et al [3] studied this problem by considering unsteady heat conduction to a particle under suddenly changing plasma conditions. They found out that the relaxation time is approximately 1.0 microsecond, which is far less than typical residence times (1.0 millisecond). Based on this finding, they concluded that the steady-state expressions for describing plasma to particle heat transfer are still valid, and they can be used for calculating heat and mass transfer coefficients.

- *Temperature Dependent Properties*

In reality, there is a large temperature drop across the boundary layer so that correction factors for convective heat and drag coefficients derived for constant properties are required. For heat transfer, the formula for the Nusselt number was modified as follows:

(i) Vardelle et al [4] gave a special attention to the effect of steep temperature gradients on the variation of the property values of the plasma across the boundary layer of the particle. These were evaluated by taking the integral mean of the property between the particle surface temperature and the temperature of the plasma calculated as follows :

$$K_{avg} = \frac{1}{(T_\infty - T_w)} \int_{T_w}^{T_\infty} K \, dT$$

A similar equation was used to evaluate μ_{avg} and ρ_{avg}. The Nusselt number was estimated using the Ranz and Marshall equation (2):

$$Nu_{avg} = \left[2 + 0.514 \, Re_{avg}^{1/2}\right]$$

Where the dimensionless numbers are defined by average properties, i.e.,

$$Re_{avg} = \frac{\rho_{avg} \, u_\infty D_p}{\mu_{avg}}$$

$$Nu_{avg} = \frac{h \, Dp}{K_{avg}}$$

(ii) Lewis and Gauvin [5] upon experimental work proposed :

$$Nu = \frac{h\, D_p}{K_f} = Nu_{avg} \left(\frac{\nu_f}{\nu_\infty}\right)^n$$

Where k is the thermal conductivity and ν is the kinematic viscosity. The subscript f refers to properties corresponding to the film temperature which is the average between the surface and free stream temperatures, and the subscript ∞ refers to properties corresponding to the free stream temperature. Nu_{avg} is given by Ranz and Marshall equation. Ahmed, A.M. [6] has obtained an experimental value of n = 0.15.

(iii) Fiszdon [7] takes the Nusselt number relation given by Bird et al [8] with a correction coefficient given by Kimura et al [9] and suggested the following formula for the Nusselt number:

$$Nu = [2.0+0.6\, Re_f^{1/2}\, Pr_f^{1/3}]\left[\frac{\rho_\infty\, \mu_\infty}{\rho_w\, \mu_w}\right]^{0.6}$$

Where μ is the dynamic viscosity. The subscript w refers to properties corresponding to the wall temperature. The subscript ∞ refers to properties corresponding to free stream temperature.

(iv) Lee et al [2] proposed the expression

$$Nu = [2.0+0.6\, Re_f^{1/2}\, Pr_f^{1/3}]\left[\frac{\rho_\infty\, \mu_\infty}{\rho_w\, \mu_w}\right]^{0.6}\left[\frac{C_{p\infty}}{C_{pw}}\right]^{0.38}$$

Where C_p is the specific heat. This expression has been fitted to the data derived from computer simulations.

(v) Sayegh and Gauvin [10], in a numerical analysis, solved the steady state continuity, Navier-Stokes, and energy equations in the stream function and vorticity formulation in spherical coordinates using finite difference techniques. A general heat transfer coefficient correlation has been derived that applies equally to constant and variable property flows.

It is found that large discrepancies exist among various approaches for calculating heat transfer coefficients. This finding already indicates the need for further studies, especially for particle heat and momentum transfer under various plasma conditions in order to develop reliable relationships. At present, there are almost no experimental data available. Thus, computer simulation of the plasma flow over a sphere remains an important tool for determining heat transfer coefficients .

- Non-Continuum Effect

The non-continuum effect on heat transfer has been studied by Chen and Pfender [1] in the temperature jump regime. They found that the non-continuum effect becomes substantial for small particles. Therefore, it is crucial for modeling associated with thermal plasma processing when small particles (< 20 micrometer) are involved. This effect can be taken into account using different accommodation coefficients for electrons and heavy particles [1].

- Radiation Transport

Radiation loss by electrons is mainly due to Bremsstrahlung radiation. Radiation losses from particle are negligible except for particles with surface temperatures exceeding 2000 °K immersed into plasmas (for example, Argon or Nitrogen) at temperatures below 4000° K [3].

- Particle Shape Effects

Both particle shape and orientation may have large effects on the rate of heat and mass transfer. There are, however, no suitable correlations available to take these effects into account, in particular for plasma heat transfer.

- Particle Charging

A particle injected into a thermal plasma is always negatively charged due to different thermal velocities and mobilities of electrons and ions.

The dimensionless surface potential (<0) is given by [2]

$$X_p = \frac{e\, \phi_p}{K_B\, T_w} = \frac{1}{4}\ln\left[\left(\frac{T_i}{T_e}\right)\left(\frac{m_e}{m_i}\right)\right]$$

Where ϕ_p, T_w, T_i, m_e and m_i are the surface

potential (< 0), surface temperature, ion temperature, electron temperature,, electron mass and ion mass; respectively. The energy transport equations taken from references (11) and (12) assume the following forms:

For neutral atoms:

$$q_{atom}=n_a\frac{2K_B^{3/2}T_{jump}^{1/2}}{\sqrt{2\pi m_a}}(T_{jump}-T_w) \quad (1)$$

For ions:

$$q_{ion}=n_i\frac{(K_BT_{jump})^{1/2}}{\sqrt{2\pi m_i}}(1-X_p+0.5X_p^2)(2K_BT_{jump}) - 2n_i\frac{(K_BT_w)^{3/2}}{\sqrt{2\pi m_a}}(\frac{T_{jump}}{T_w})^{1/2} \quad (2)$$

For electrons:

$$q_e=n_e\frac{(K_BT_{e\ jump})^{1/2}}{\sqrt{2\pi m_e}}(2K_BT_{e\ jump})\ \exp(X_p) \quad (3)$$

Recombination between ions and electrons:

$$q_{recom}=n_i\frac{(K_BT_{jump})^{1/2}}{\sqrt{2\pi m_i}}E_i\exp(-X_p) \quad (4)$$

Where, the q's represent the heat fluxes, T_{jump} and $T_{e\ jump}$ are the jump temperatures, T_w is the particle surface temperature, the m's are the molecular masses of the species and E_i is the recombination energy.

ANALYTICAL MODEL AND THE GOVERNING EQUATIONS

The basic assumptions of the model are:

(1) The flow is steady and axisymmetric;
(2) Gravity and viscous dissipation have been neglected;
(3) There are no superimposed fields (neither electric nor magnetic);
(4) Electron diffusion is controlled by ambipolar diffusion;
(5) Radiation losses are included in the electron energy equation;
(6) Electron-electron-ion collisions are the only process for volume recombination.

Then the governing equations can be written as follows:

- Conservation of Mass Equations

Continuity Equation for All Species :

$$\nabla.(\rho\ U) = 0 \quad (5)$$

Where ρ is the density of all species which can be taken equal to the density of heavy particles because of the low electron number density and its light mass, and U is the velocity vector.

Continuity Equation for Electrons :

$$\nabla.(\rho_e\ U)=\nabla.\rho\ D_{amb}\ \nabla(\rho_e/\rho) + m_e\ \dot{n}_e \quad (6)$$

Where ρ_e, D_{amb}, m_e and $\dot{n}_e$ are the electron mass density, ambipolar diffusion coefficient, electron mass and the ionization rate , respectively.

- Momentum Equations

r - Direction Momentum Equation :

$$\rho[u_r\frac{\partial u_r}{\partial r}+\frac{u_\theta}{r}\frac{\partial u_r}{\partial\theta}-\frac{u_\theta^2}{r}]= -\frac{\partial P}{\partial r} +\frac{\partial}{\partial r}[2\mu\frac{\partial u_r}{\partial r}-\frac{2\mu}{3}(\nabla.U)] +\frac{1}{r}\frac{\partial}{\partial\theta}[\mu(r\frac{\partial}{\partial r}(\frac{u_\theta}{r})+\frac{1}{r}\frac{\partial u_r}{\partial\theta})] +\frac{\mu}{r}[4\frac{\partial u_r}{\partial r}-\frac{2}{r}\frac{\partial u_\theta}{\partial\theta}-\frac{4u_r}{r}-\frac{2u_\theta\cot\theta}{r} +r\cot\theta\frac{\partial}{\partial r}(\frac{u_\theta}{r})+\frac{\cot\theta}{r}\frac{\partial u_r}{\partial\theta}] \quad (7)$$

θ- Direction Momentum Equation :

$$\rho[u_r\frac{\partial u_\theta}{\partial r}+\frac{u_\theta}{r}\frac{\partial u_\theta}{\partial\theta}+\frac{u_r\ u_\theta}{r}] = -\frac{1}{r}\frac{\partial P}{\partial\theta} +\frac{1}{r}\frac{\partial}{\partial\theta}[\frac{2\mu}{r}(\frac{\partial u_\theta}{\partial\theta}+u_r)-\frac{2\mu}{3}(\nabla.U)] +\frac{\partial}{\partial r}[\mu(r\frac{\partial}{\partial r}(\frac{u_\theta}{r})+\frac{1}{r}\frac{\partial u_r}{\partial\theta})] +\frac{\mu}{r}[2(\frac{1}{r}\frac{\partial u_\theta}{\partial\theta}-\frac{u_\theta\cot\theta}{r})\cot\theta +3(r\frac{\partial}{\partial r}(\frac{u_\theta}{r})+\frac{1}{r}\frac{\partial u_r}{\partial\theta})] \quad (8)$$

In Eqs. (5) to (8) the usual symbols employed in fluid mechanics are used; r and θ are the radial and circumferential coordinates, u_r and u_θ are the velocity components in these directions, respectively; P and μ are the gas pressure and dynamic viscosity.

- Energy Equations

Heavy Particle Energy Equation :

$$\nabla.[\frac{5}{2} K_B n_h T U] = \nabla.K_h \nabla T + Q_{eh} \quad (9)$$

Electron Energy Equation :

$$\nabla.[\frac{5}{2} K_B n_e T U] = \nabla.K_e \nabla T_e - E_i \dot{n}_e - R - Q_{eh} \quad (10)$$

Where K_B is the Boltzmann's constant and n_h, n_e, T, T_e, K_h and K_e are the number density of heavy particles, number density of electrons, heavy particle's temperature, electron's temperature, thermal conductivity of heavy particles and thermal conductivity of electrons respectively, E_i, R and Q_{eh} are the ionization energy, radiation loss from electrons and energy transfer from the electrons to heavy species.

The energy transfer from electrons to heavy species through collision processes, Q_{eh}, are the sum of the electron-ion energy transfer, Q_{ei}, and electron-neutral energy transfer, Q_{ea} [13].

$$Q_{ei} = \frac{2 n_e n_i e^4}{3 m_h (4\pi\epsilon_o)^2} [\frac{8\pi m_e}{K_B T_e}]^{1/2} \frac{T_e - T}{T_e} \ln[\frac{9(4\pi\epsilon_o K_B T_e)^3}{4\pi n_e e^6}] \quad (11)$$

Where e is the elementary charge and m_h is the mass of heavy particle and ϵ_o is the permitivity of vacuum.

$$Q_{ea} = 3K_B(T_e - T) n_e \frac{m_e(1-\alpha)\rho}{m_h^2} * [\frac{8\pi m_e}{K_B T_e}]^{-1/2} \sigma_{ea} \quad (12)$$

Where α, σ_{ea} are the degree of ionization, and the electron-neutral elastic collision cross section respectively.

Radiation loss from electrons can be assumed to be due to Bremsstrahlung radiation [14].

$$R = 1.69 * 10^{-26} n_e n T_e^{1/2} \text{ (watt m}^{-3}) \quad (13)$$

In Eqs. (5) - (13), spherical coordinates (r,θ,Φ) are employed, and both steady state$(\partial/\partial t=0)$ and axisymmetric $(\partial/\partial\Phi=0)$ are postulated.

- Equation of State

Considering Argon as an ideal gas, the pressure of the plasma is given by :

$$P = \rho R T \quad (14)$$

Where R is the gas constant .

-Boundary Conditions

Far from the sphere $(r=\infty)$, the free stream conditions are :

$$\alpha=\alpha_\infty \;,\; u_r=-u_\infty \cos(\theta),\quad u_\theta=-u_\infty \sin(\theta),\quad T=T_\infty \text{ and } T_e=T_{e\infty} \quad (15)$$

Where the subscript ∞ refers to the free stream conditions.

At the sphere surface, slip velocity and temperature jump boundary conditions are used as:

$$u_{\theta s} = \frac{2-f}{f} \lambda \frac{\partial u_\theta}{\partial r} \quad (16\text{-a})$$

$u_r=0$ impermeable surface B.C. (16-b)

$$T_s = T_w + \frac{2-a}{a} \frac{2\gamma}{\gamma+1.0} \frac{\lambda}{Pr} \frac{\partial T}{\partial r} \quad (16\text{-c})$$

$$T_{es} = T_{ew} + \frac{2\gamma}{\gamma+1.0} \frac{\lambda_e}{Pr_e} \frac{\partial T_e}{\partial r} \quad (16\text{-d})$$

Where λ, λ_e, f, a, and subscripts s and w denote the mean free path length of heavy particles, of

electrons, momentum and thermal accommodation coefficients, and jump and surface conditions, respectively. Note that " a " is assumed to be 1 for the electrons. Here, the boundary condition for the electron density has been derived using the following approach;

$$\frac{<c>}{4}\alpha_s = \frac{D_{amb}}{2}\frac{\partial \alpha}{\partial r} \qquad (16\text{-e})$$

where α and <c> are the degree of ionization and the average thermal velocity, respectively .
Along the axis of symmetry (θ=0° and θ=180°):

$$\frac{\partial \alpha}{\partial \theta}=0,\quad \frac{\partial u_r}{\partial \theta}=0,\quad u_\theta=0,\quad \frac{\partial T}{\partial \theta}=0,\quad \frac{\partial T_e}{\partial \theta}=0. \qquad (17)$$

NUMERICAL DATA:

For all the computational work described in this study, the particle diameter is 20μm, the thermal accommodation coefficient, (a), is taken as 0.8 according to reference (1), the momentum accommodation coefficient, (f), is 0.9 according to the same reference, T_∞ is 13000°K, and $T_{e\infty}$ is 13000°K too. The particle surface temperature T_w is 1000°K. The Prandtl number for Argon is constant and equal to 0.651 whereas the Prandtl number for electrons is found to be 0.644691.

The degree of ionization far from the sphere is calculated from Saha Equation as the plasma is in (LTE). Reynolds number is taken to be 1.0, or less sometimes, and the specific heat ratio is equal to 1.67.

METHOD OF SOLUTION

Normalization

The governing equations are normalized by introducing new variables, properties and coordinate, non dimensionalized in terms of the bulk conditions of the gas and the sphere radius (D/2), thus:

$$\rho^*=\frac{\rho}{\rho_\infty}\quad \alpha=\frac{n_e}{n_\infty}\quad u_r^*=\frac{u_r}{u_\infty}\quad u_\theta^*=\frac{u_\theta}{u_\infty}\quad T^*=\frac{T}{T_\infty}\quad T_e^*=\frac{T_e}{T_\infty}$$
$$r^*=\frac{r}{(D/2)}\quad D_{amb}^*=\frac{D_{amb}}{D_{amb\infty}}\quad \mu^*=\frac{\mu}{\mu_\infty}\quad K_h^*=\frac{K_h}{K_{h\infty}}\quad K_e^*=\frac{K_e}{K_{h\infty}} \qquad (18)$$

The new coordinate z is introduced in a way such that $r^*=e^z$, to represent radial distance. The new dimensionless radial distance,z,allows exponential increase in r for equal increments of z. Also, when z is used, the radial spacing near the surface of the sphere is kept small to improve the accuracy of calculation, while still maintaining a relatively large domain with a reasonable number of mesh points.

Linearization Method Of Difference Equations

For the numerical prediction method considered here, the nonlinear equations were transformed from their original partial differential form to a set of nonlinear algebraic equations, thus, making them amenable to a computer solution. To do this, the flow field was first divided into a large number of mesh points. The variables, at each of these points, were approximated by Taylor series and the derivatives were determined in terms of adjacent points. The solution, then, consisted of satisfying the difference equations at every lattice point. The central difference method was used for all of the internal points. With this method, the derivative is approximated by the difference between points on both sides of the point under consideration. Forward difference and backward difference approximations evaluate the derivatives in terms of two or more consecutive points in the same direction, either in front or behind the lattice point. These were used to approximate the Neumann-type boundary conditions. The general finite-difference equations, accurate up to the order of h^2 are given in appendix of reference(16).

Figure (1) illustrates the circular mesh used. It can be seen that the divisions are smaller near the surface of the sphere. This was necessary for

obtaining accurate description of the flow where the gradients are steepest. They go larger as r increases.

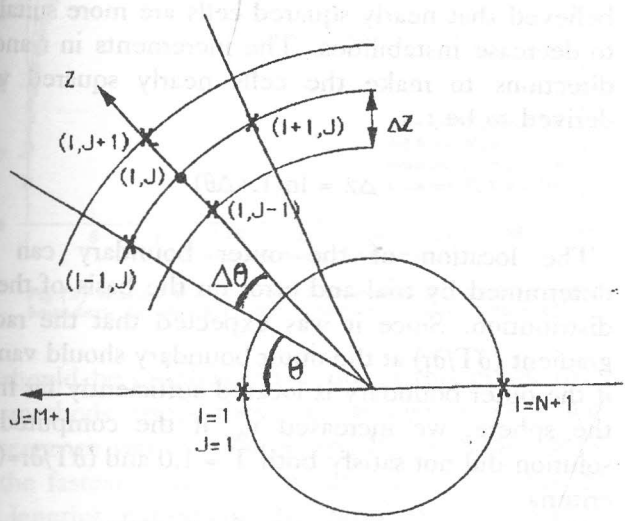

Figure 1. Circular mesh θ vs. Z.

Flow predictions are then based on the solution of the set of nonlinear algebraic equations. This solution can be obtained by iteration using the following procedure :

(1) the equations are linearized based on the best estimate for the dependent variables.
(2) the linear equations are "solved" to improve the estimate for the solution.
(3) this " coefficient update cycle " is repeated until the solution obtained satisfies the nonlinear equations to a specified tolerance.

The accuracy of the linearizations used affects the rate of convergence of the linear equation solutions [15]. More accurate linearizations generally accelerate the convergence rate at the expense of the time required for the solution of the linear equation set.

Standard Linearization [15]: This first-order-accurate linearization is desirable so that solution of the linear equation set becomes simple. A linear equation can be solved for a new estimate of its variable, independent of other equations. This new estimate of the variable can then be used in another equation and so on. This linearization does not accurately mimic the physics of the flow, with the result that heavy under-relaxation is required to avoid divergence.

Newton-Raphson Linearization [15] : If a more accurate linearization is employed, such as a Newton-Raphson linearization, where nonlinear terms are approximated by the first two terms of a Taylor series expansion, for example, the uT product results in :

$$uT = u^{o} T + T^{o} u - u^{o} T^{o} \qquad (19)$$

Where the superscript o denotes the values from the previous updated cycle. Then, the linear equations are coupled directly to each-other. The convergence rates of the nonlinear set achieved through solution of this equation set have been shown to be significantly higher than those possible with the standard linearization, i.e., the number of coefficient update cycles is lower than that in the standard linearization. Unfortunately, the increased computational effort required to solve each coupled linear equation set by existing means outweighs the savings that result from the accelerated convergence rate.

In the present study, we shall make use of both the Newton-Raphson linearization method to "first" linearize the algebraic equations, and the standard linearization method to "secondly" solve the previous coupled linear equation set. This permits the use of both accurate linearization method and simple faster method for conversion.

The Relaxation Procedure

Equations (12) to (16) can be written in a general form as:

$$\phi(I,J)=f\ [\phi(I+1,J),\phi(I-1,J),\phi(I,J+1),\phi(I,J-1)] \qquad (20)$$

Hence, to find the value of the function ϕ at the point (I,J), the values of this function must be defined for the four adjacent points. In other words, to start the process, initial values for all the functions at every mesh point in the grid must be assigned. To satisfy the governing equations, new values of the variable are then calculated with the aid of equation (20). If the initial guess was very far from the required solution, then direct substitution of the new values in the grid can cause instabilities which may lead to divergence of the solution from actual values. To avoid this, the new value of the function that is placed in the grid is chosen between the old and the calculated values, thus :

$$\phi_{new} = \phi_{old} + w^*(\phi_{cal} - \phi_{old}) \quad (21)$$

w is known as the relaxation coefficient. When w is greater than unity, the method is called Over Relaxation and if w is less than unity the method is called Under Relaxation.

Either of two methods can be used to evaluate equation (21):

(a) Richardson's method where the old values for all of the variables are used to evaluate ϕ, or;

(b) Liebmann's method where the new values are used as they are calculated.

Richardson's method was used in this study.

Usually, the selection of the relaxation coefficient is based on the highest value that does not cause instabilities .

In this study, three relaxation coefficients (w_1,w_2,w_3) were used for the degree of ionization, velocities and temperatures. Small values of (w_1,w_2 and w_3) were used at the start and then they were permitted to increase every 20 iterations to accelerate convergence. The values of (w_1,w_2 and w_3) at the start were 0.4, 0.4 and 0.5; respectively.

A computer program was written for the simultaneous solution of the governing equations by the above iteration method. Direct substitution and constant relaxation coefficients were applied alternately on the mesh points to calculate the new values of the variables.

Computation Sequence

The number of iterations required to reach convergence depends on the nature of the problem, the relaxation coefficients used and on the initial guess. Starting with a guess that was far from the real solution for the condition under study caused instabilities and required the use of heavy-under-relaxation coefficients which in turn led to an increase in the number of iterations.

From a computation point of view, the direct effect of increasing field size and reducing lattice spacing is an increase in the computer memory and in the time required per iteration. Decreasing the field size may cause inaccuracies and instabilities in the solution, especially at the rear part of the sphere.

No systematic investigation of the exact effects of lattice spacing and field size on the accuracy of the solutions, in order to permit the selection of an optimum mesh, was found in the literature.

In this work, where central difference is used, it is believed that nearly squared cells are more suitable to decrease instabilities. The increments in r and θ directions to make the cells nearly squared was derived to be :

$$\Delta z = \ln(1.+\Delta\theta)$$

The location of the outer boundary can be determined by trial and error on the basis of the T distribution. Since it was expected that the radial gradient ($\partial T/\partial r$) at the outer boundary should vanish if the outer boundary is located sufficiently far from the sphere, we increased r_∞ if the computed T solution did not satisfy both T = 1.0 and ($\partial T/\partial r$=0.0) criteria.

Numerical experiments of increasing r_∞ were performed until ($\partial T/\partial r$) becomes smaller than a predetermined small number ϵ. Figure (2) illustrates this trial-and-error effort where ϵ was taken as 10^{-3}. For the specified parametric values, it is seen that choosing r_∞ to be 19.14 times the sphere radius is adequate.

The initial guess for velocities were the creeping flow distribution. For temperatures :

$$T(I,J) = (1 - e^{-r})-0.001\theta \quad (22)$$

$$T_e(I,J)= (1 - e^{-r})-0.001\theta \quad (23)$$

where θ is in radians.

Since the degree of ionization is proportional to the electron temperature, the initial guess for α can be assumed as:

$$\alpha(I,J) = \alpha_\infty(1 - e^{-r})-0.001\theta \quad (24)$$

The convergence criterion in this study was based on maximum absolute error in all variables. When the change in these variables between successive iterations was less than the tolerance, at every lattice point, the computation process was stopped and the required quantities were calculated. The tolerance was taken as 10^{-3}.

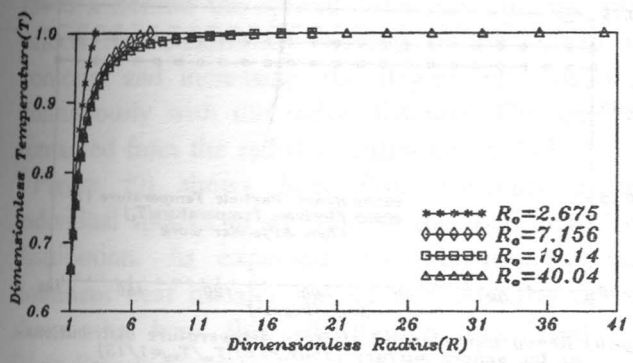

Fig.(2) Radial temperature distribution for various outer boundary locations of the spherical domain (angle=45°)

It should be emphasized again, at this point, that the methods used above to accelerate or reach convergence were very arbitrary. By no means, they are the fastest or the " optimum " ones. Because of the lengthy nature of the problem, it was not possible to investigate the methods of solution systematically and come up with definite recommendations on the best method that should be used.

RESULTS DISCUSSION AND CONCLUSIONS

A code using the proposed model is written and a system of program runs was performed and the results are to be presented and explained below.

Figures (3) and (4) show the isotherms of heavy particles and electrons respectively. The isotherm distributions in each figure are determined by the interplay of the heat conduction and the imposed convection.

Ahead of the sphere, the heat conduction and convection are concurrent, therefore, the isotherm distributions are dense to a certain extent there, while behind the sphere, the convection is in opposite direction with respect to conduction and hampers the heat transfer by conduction so that the isotherms spread somewhat downstream.

The previous effects can be noticed in figure (4) but it may be hard to recognize in Figure (3). This is because in low Reynolds number regimes, such as our case where Re = 1.0, the isotherms appear symmetrical to a certain extent with respect to x=0.0. The symmetricity feature is expected to be more obvious as Re is lowered. Complete symmetry is achieved when Re=0, which corresponds to the pure heat conduction problem in a stagnant gas. The effect of spreading the electron temperature isotherms in the downstream region is remarked, but not for the heavy particle temperature isotherms because of the higher mobility of electrons than that of heavy particles.

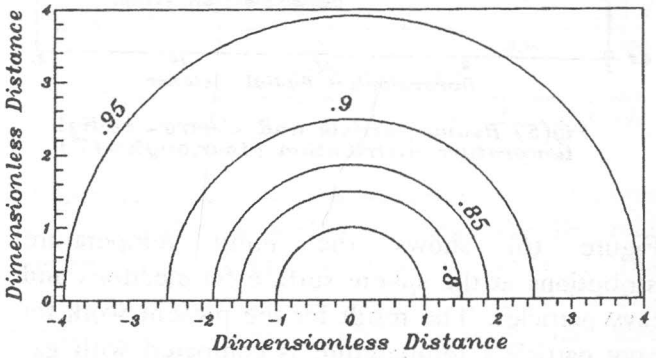

Fig.(3) Heavy particle dimensionless temperature field around a sphere (1bar,Re=1,T_w/T_{∞}=1/13)

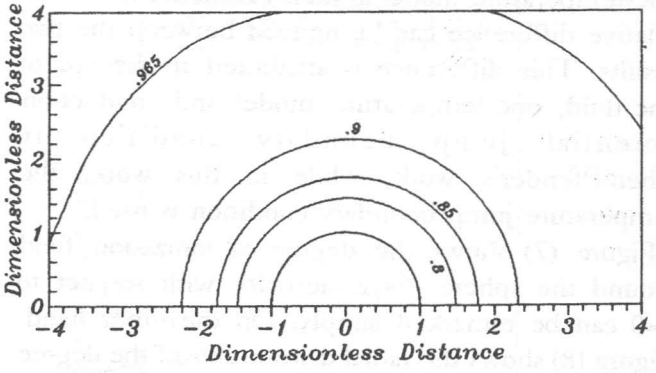

Fig.(4) Electron dimensionless temperature field around a sphere(1bar,Re=1,T_w/T_{∞}=1/13)

Figure (5) shows the radial temperature distribution for electrons and heavy particles at (θ=45°). Except near the sphere surface, the temperature of electrons shows higher values than that of heavy particles, however, both of the electron and heavy particle temperatures decrease slowly in the negative r-direction. Near the sphere surface, both of the two temperatures decrease rapidly since the sphere represents a sink of heat. Because of the higher thermal accommodation coefficient of electrons than that of heavy particles, the electron temperature goes down to a lower value at the sphere surface than that of the heavy particles.

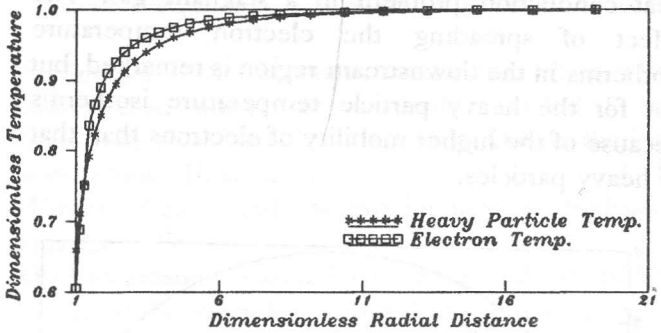

Fig(5) Heavy particle and electron radial temprature distribution (1bar,angle=45°)

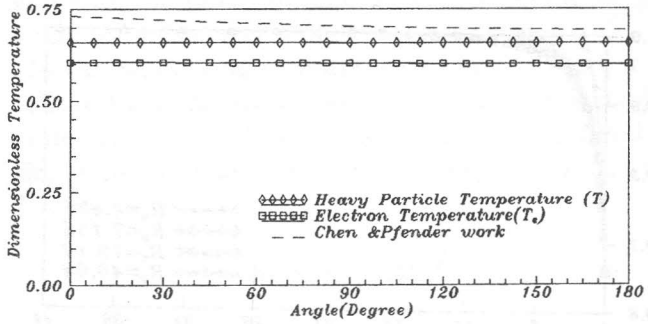

Fig.(6) Heavy particle and electron temperature distributions at the sphere surface (1bar,Re=1,$T_w/T_{\infty f}$=1/13)

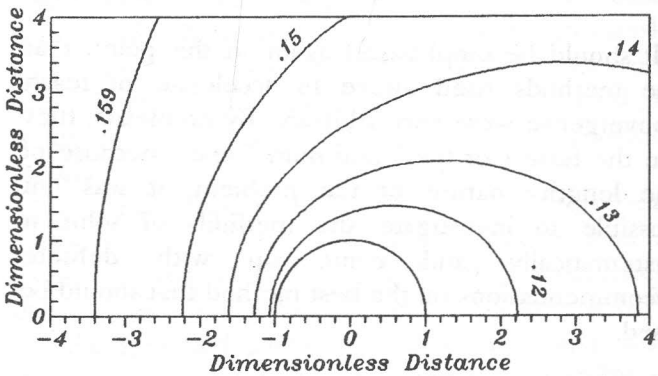

Fig.(7) Degree of ionization around a sphere (1bar,$T_w/T_{\infty f}$=1/13,Re=1)

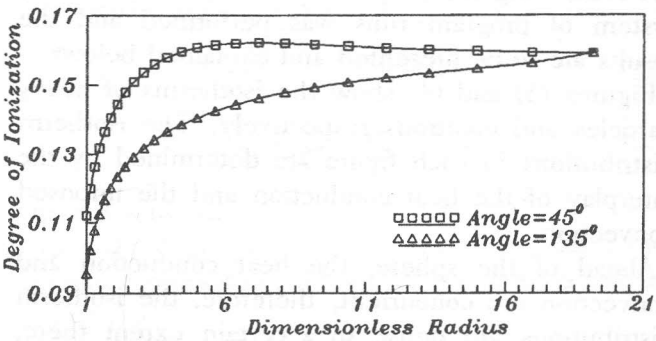

Fig.(8) Degree of ionization radial distribution in the rear and the front of the sphere (1bar)

Figure (6) shows the jump temperature distributions at the sphere surface for electrons and heavy particles. The result for the present work for heavy particle's temperature is compared with gas jump temperature given by Chen and Pfender in reference (1). Chen and Pfender used one-fluid, one-temperature model in their calculations. A small relative difference can be noticed between the two results. This difference is attributed to the use of one-fluid, one-temperature model and conduction potential jump boundary condition in Chen-Pfender's work, while in this work, the temperature jump boundary condition is used.

Figure (7) shows the degree of ionization field around the sphere. Asymmetricity with respect to x=0 can be remarked simply. On the other hand, Figure (8) shows the radial distribution of the degree of ionization ahead (θ=45°) and behind (θ=135°) the sphere. The two factors affect the degree of ionization distribution, namely, the electron temperature and convection. The degree of ionization is proportional to the electron temperature, while the convective flow carries electrons in its direction. The curve of electron temperature radial distribution can be divided into two regions; the first region lies far from the sphere and over which the electron temperature decreases slowly with decreasing the radial distance; while the second region lies nearby the sphere surface in which the electron temperature decreases rapidly with high slope with decreasing the radial distance. The two regions are connected by a smooth knee at about six times the sphere radius.

Ahead of the sphere (upstream), the convection and temperature effects have opposite directions. In the first region, the effects of convection overcomes the temperature effect leading to increase in the degree of ionization in the direction of the sphere up to the knee. In the second region, the temperature effect overcomes the convective effect leading to changing the sign of the slope of the degree of ionization curve. This change in sign explains the overshooting noticed in the radial distribution at

(θ=45°). Behind the sphere (downstream), the two effects act concurrently leading to the spread of contours and increasing the degree of ionization continuously with the radial distance. This can be remarked from the radial distribution at (θ=135°).

Figure (9) shows heat flux distributions by individual species in addition to the total heat flux distribution. As expected, recombination is the dominant heat transfer mechanism. Also,the figure shows the heat flux distribution calculated by Chen-Pfender in reference (1), where conventional heat conduction by temperature gradient was adopted. The difference between the results of this study and Chen-Pfender's work agrees well with our expectancy that small particle diameters, non-equilibrium nature of the boundary layer and surface charging will have strong effects on the heat transfer mechanisms.

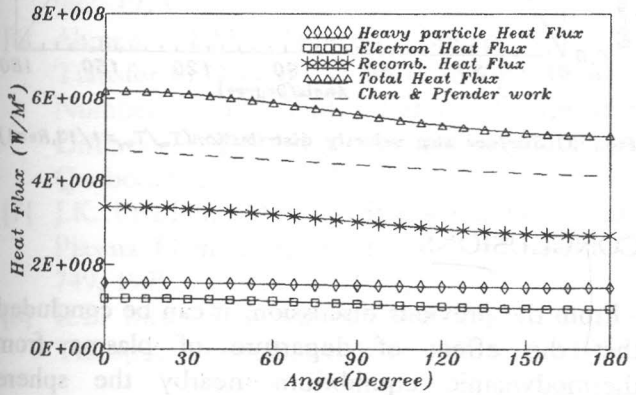

Fig.(9) Heat fluxes distribution at the sphere surface by individual species (1bar,Re=1,T_w/T_{wf}=1/13)

Figure (10) shows the total and the individual species contribution to the heat flow into the sphere at different pressures. When pressure is decreased, both the number density of heavy particles and the number density of electrons are decreased with the result that each contribution is decreased too. However, it may be noticed that recombination heat flow is dominant and considerably greater than that of heavy particles or electrons. It is obvious from the figure that the relative importance of electron heat flow is increased because of the increase of the degree of ionization.

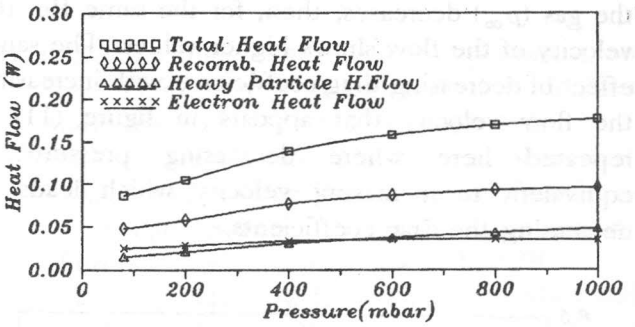

Fig.(10) Heat flow in by individual species for different pressures (D=20 mic,Re=1,T_w/T_{wf}=1/13)

Figure (11) shows the variation of friction, pressure and the total drag coefficients with the Reynolds number. The qualitative trend is similar to that calculated by Sayegh and Gauvin[10] where the drag coefficients decrease with increasing the flow velocity.

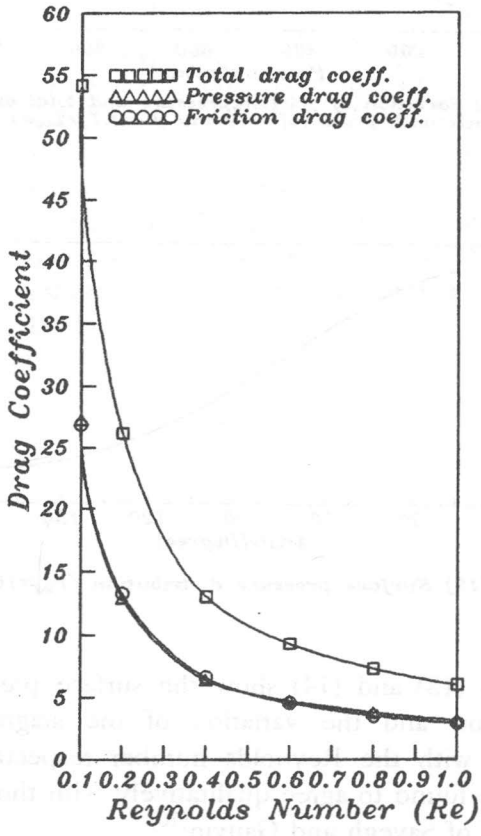

Fig(11)Variation of friction , pressure and total drag coefficients with Re

Figure (12) shows the variation of friction, pressure, and total drag coefficients with pressure at Re = 1. As the pressure decreases, the density of the bulk of

the gas (ρ_∞) decreases, then, for the same Re, the velocity of the flow shows higher values. The same effect of decreasing drag coefficients with increasing the flow velocity that appears in figure (11) is repeated here where decreasing pressure is equivalent to increasing velocity which leads to decreasing the drag coefficients.

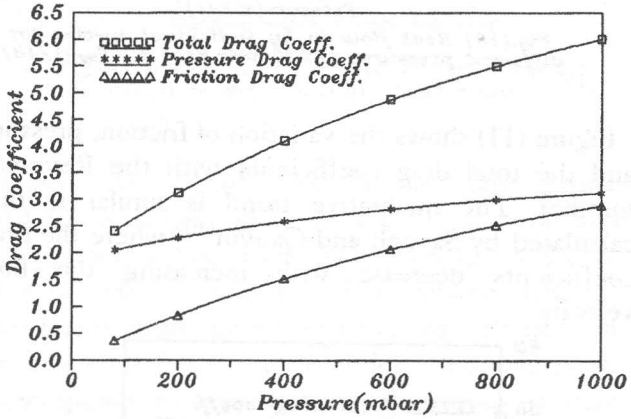

Fig.(12) Variation of friction,pressure and total drag coefficients with pressure(D=20 mic.,Re=1,T_w/T_{wf}=1/13)

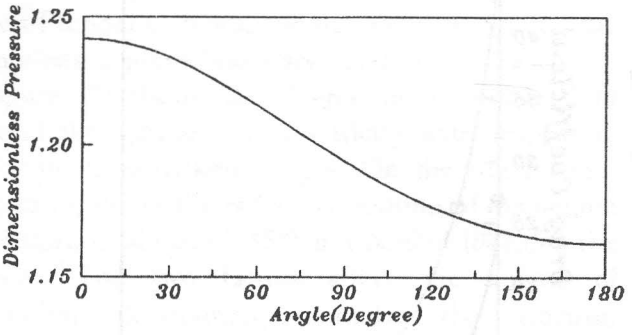

Fig.(13) Surface pressure distribution (P_{wf}=1bar)

Figures (13) and (14) show the surface pressure distribution and the variation of the stagnation pressure with the Reynolds number respectively. They are found to agree qualitatively with those in the work of Sayegh and Gauvin[10].

Figure (15) shows the surface slip velocity distribution. It shows the same behavior of the work done by Chen and Pfender[10].

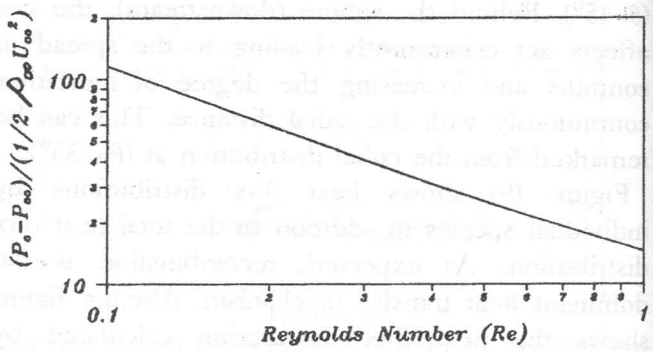

Fig(14) Variation of front stagnation pressure P_o with Reynolds number Re

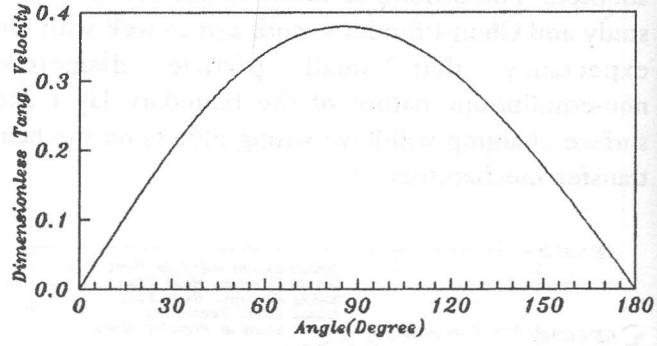

Fig.(15) Surface slip velocity distribution(T_w/T_{wf}=1/13,Re=1)

CONCLUSIONS

From the previous discussion, it can be concluded that the effect of departure of plasma from thermodynamic equilibrium nearby the sphere surface has a recognized effect on the resultant heat fluxes.

Considering the fact that recombination heat flow is the dominant mode of heat flow near the sphere surface, the boundary layer non-equilibrium characteristics should be taken into account.

The one-fluid, one-temperature model underestimates the calculated heat flows from the plasma to the sphere surface. This is due to the fact that one-fluid, one-temperature model overlooks the contribution of both electrons and recombination energy.

The difference in estimated heat flux using this model and the one fluid one temperature model is about 20% .

REFERENCES

[1] X. Chen and E. Pfender," Behavior of Small Particles in a Thermal Plasma Flow", *Plasma Chem. Plasma Process.* 3, 351, 1983.

[2] Y.C.Lee, Y.P. Chyou and E. Pfender ," Particle Dynamics and Particle Heat and Mass Transfer in Thermal Plasmas. Part II: Particle Heat and Mass Transfer in Thermal Plasmas", *Plasma Chem. Plasma Process.* 5, 391, 1985.

[3] E. Bourdin, P. Fauchais and M. I. Boulos, "Transient Heat Conduction under Plasma Conditions" *Int.J. Heat Mass Transfer*, 26, 567, 1983.

[4] M. Vardelle, A. Vardelle, P. Fauchais and M.I. Boulos," Plasma-Particle Momentum and Heat Transfer: Modeling and Measurements", *AIChE J.* 29, 236, 1983.

[5] J.A. Lewis and W.H. Gauvin, "Motion of Particle Entrained in a Plasma Jet", *AIChE J.* 19, 982, 1973.

[6] Ahmed, A.M., "Forced Convective Heat Transfer to Cooled Cylinders at Low Reynolds Numbers and With Large Temperature Difference", *T.N. 67-5, McGill Univ.*, Montreal, Quebec, Canada, 1967.

[7] J.K. Fiszdon, "Melting of Powder Grains in a Plasma Flame", *Int. J. Heat Mass Transfer*, 22, 749, 1979.

[8] R.B. Bird, W.E. Stewart and E.N. Lightfoot, Transport Phenomena, *Wisconsin Univ.*, 1960.

[9] I. Kimura and A. Kanzawa, "Experiments on Heat Transfer to Wires in a Partially Ionized Argon Plasma", *AIAA J. 3*, 476-481, 1965.

[10] N.N. Sayegh and W.H.Gauvin,"Numerical Analysis of Variable Property Heat Transfer to a Single Sphere in High Temperature Surroundings", *AIChE J.* 25, 522, 1979.

[11] N.N. Rykalin, A.A. Uglov, Yu.N. Lokhov and A.G. Gnedovets, "Properties of Heating of Submicron Metal Particles in a Hot Gas", *High Temp.* 19, 404, 1981.

[12] X. Chen, Y.C. Lee and E. Pfender, "The Importance of Knudsen and Evaporation Effect", *6th International Symposium on Plasma Chemistry*, Montreal, Canada, 1983.

[13] M. Hoffert and H. lien, *Phys. Fluids* 8, 1608, 1965.

[14] David L. Book, *NRL.* Plasma Formulary, 1987.

[15] P.F. Galpin and G.D. Raithby, "Numerical Solution of Problems in Incompressible Fluid Flow : Treatment of the Temperature-Velocity Coupling", *Numer. Heat Transfer*, vol. 9, pp. 105-126, 1986.

[16] Mofreh R. Zaghloul,"Heat and momentum transport in plasma flow around a solid sphere", Master thesis, Alexandria University, 1994.